NUMERICAL INVESTIGATION OF FLOW AND THERMAL PATTERN IN UNBOUNDED FLOW USING NANOFLUID (Case study: Laminar 2-D Plane Jet)

by

Taher ARMAGHANI [a]*, Mohammad Javad MAGHREBI [b], Farhad TALEBI [c], and A. BAQAIE SARYAZDI [c]

[a] Department of Engineering, Mahdishahr Branch, Islamic Azad University, Mahdishahr, Iran
[b] Department of Mechanical Engineering, Ferdowsi University of Mashad, Mashhad, Iran
[c] Department of Mechanical Engineering, Semnan University, Semnan, Iran

Original scientific paper
DOI:10.2298/TSCI130330120A

In this article, a numerical study is carried out to analyze the effect of nanoparticle volume fraction over flow and thermal characteristics of laminar 2-D plane jet. Al_2O_3-water and TiO_2-water nanofluids are considered in this investigation with lowest and highest values of particle volume concentration equals to 0 and 0.02, respectively. This paper propose four correlations for describing the relation between the solid volume fraction, δ_T and δ_U. The results show that the cross stream thermal diffusion depth and cross stream hydraulic diffusion depth are increased when particles volume concentration is increased and mean temperature and mean velocity decreases when the solid volume fraction is increased. The effects of nanoparticle volume fraction in velocity and temperature time histories are also studied and discussed.

Key words: *nanofluid, nanoparticle volume fraction, cross stream thermal diffusion depth, cross stream hydraulic diffusion depth*

Introduction

Nanofluids, a name conceived by Choi [1] in Argonne National Laboratory, are fluids consisting of solid nanoparticles with size less than 100 nm suspended with solid volume fraction typically less than 4%. Nanofluids can enhance heat transfer performance compared to pure liquids. Nanofluids can be used to improve thermal management system in many engineering applications such as transportation, micromechanics and instrument, HVAC systems and cooling devices [2]. Recently, many investigators studied nanofluid convective heat transfer in different geometries both numerically and experimentally [3-7]. For numerical simulation, two approaches have been adopted in the literature to investigate the heat transfer characteristics of nanofluids, single phase model and two phase model. Another approach is to adopt the Boltzmann theory [8]. In single phase model, a uniform volume fraction distribution is assumed for nanofluids. In other words, the viscosity and thermal conductivity of nanofluids are formulated by volume fraction and nanoparticle size then continuity, momentum and energy equations are solved for nanofluids. In two phase model, the volume fraction distribution equation is added to other conservation equations. Many investors used single and two phase models for investigating the flow and heat transfer of nanofluids [9-11].

* Corresponding author; e-mail: taherarmaghani@yahoo.com

A numerical investigation of laminar mixed convection flow through a copper-water nanofluid in a square lid-driven cavity has been studied by Talebi *et al.* [12]. They showed the effect of solid concentration as a positive effect on heat transfer enhancement.

A numerical investigation of mixed convection flows through a copper-water nanofluid in a square cavity with inlet and outlet port has been performed by Shahi *et al.* [13]. The results indicated that any increase in solid concentration leads to an increase in the average Nusselt number at the heat source surface and a decrease in the average bulk temperature.

The effective assessment of aluminia nanoparticle at enhancing single-phase and two-phase heat transfer in micro-channel heat sinks has been performed by Lee and Mudavar [14]. The high thermal conductivity of nanoparticles was shown to enhance the single-phase heat transfer coefficient. However, the enhancement was weaker in fully developed region. It proved that nanoparticles have an appreciable effect on thermal boundary layer development.

The effects of nanoparticle volume fraction in hydrodynamic and thermal characteristics of forced plane jet are studied by Maghrebi *et al.* [15]. The results showed nanoparticle volume fraction has a significant role in hydrodynamic and thermal characteristics of forced plane jet. The results for both nanofluids indicated that any increase in the solid volume fraction decreases the amplitude of temperature and velocity time history, the turbulent intensities and Reynolds stresses. The results for both two nanoparticles also indicated that with any increase in nanoparticle volume fraction, the velocity amplitude of velocity time history, the turbulent intensities and Reynolds stress in Al_2O_3-water are greater than that of CuO-water. This article is the extension of our previous work. In this paper, the effect of volume fraction on cross stream thermal and dynamic diffusion depth in laminar plane jet has been studied. Our previous work focused on forced plane jet and studied the turbulent intensities and Reynolds stress and other turbulent characteristic. In this work we study the effect of nanoparticle volume fraction in hydrodynamic and thermal characteristics of laminar free jet, which has very industrial application such as fusion [16, 17], vacuum environment [18] and cooling of electronic devices.

The effective thermal conductivity of nanofluid has been also calculated with a model proposed by Yu and Choi [19]. To determine the viscosity of nanofluid, two experimental correlations for Al_2O_3 and TiO_2 proposed by Nguyen *et al.* [20] and Dungthongsuk and Wongwises [21], have been used, respectively. The aim of this paper is: investigation the effects of solid volume fraction on thermal and hydrodynamic characteristics of laminar plane jet.

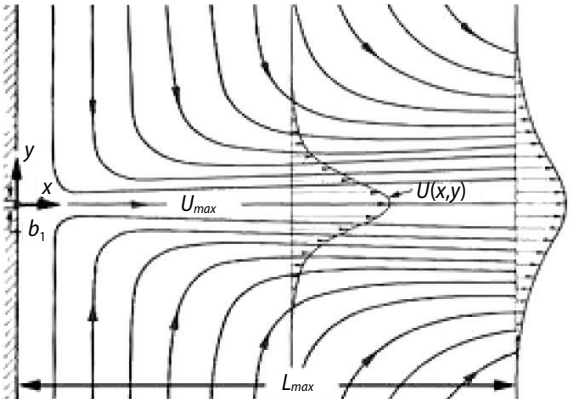

Figure 1. Spatially developing jet geometry

Mathematical modelling

Figure 1 shows the co-ordinate system and the computational domain in which the governing equation for the incompressible jet flow are solved. The inlet velocity profile is specified by $U_0(y)$ that has a superimposed computational velocity. The jet flow is allowed to be developed in the spatial direction x.

Governing equations

In this paper the governing equations are derived for the full incompressible Navier-Stokes and Energy equations. These equations together plus an equation representing mass conservation are

the governing equation for an incompressible plane jet flow. These are solved in a domain which is finite in the stream wise x-direction, and doubly infinite in the cross stream y-direction. In the x-direction a high order compact finite difference scheme is used and in the y-direction, a mapped compact finite difference method is employed. All equations are non-dimensionalized by the appropriate characteristics scale of jet. All lengths are normalized by the inlet jet half width, $b_{1/2}$, and velocities are normalized by U_{in}^{*} . Time is normalized by $b_{1/2}/U_{in}^{*}$ and temperature is normalized by T_{in}^{*} and T_{∞}^{*} as:

$$T = (T^{*} - T_{\infty}^{*})/(T_{in}^{*} - T_{\infty}^{*})$$

The mean component of the stream wise velocity at the inlet plane of the domain, is:

$$U_0(y) = \frac{1}{\cosh^2 y} \tag{1}$$

which is presented by Schlichting [22].

The computational flow velocity components $\left[u(x,y,t), v(x,y,t)\right]$ are:

$$U(x,y,t) = U_0(y) + u(x,y,t) \tag{2}$$

$$V(x,y,t) = v(x,y,t) \tag{3}$$

$$\frac{\partial}{\partial t}\nabla^2 u = \frac{\partial^2 H_1}{\partial y^2} - \frac{\partial^2 H_2}{\partial x \partial y} + \frac{1}{\mathrm{Re}}\nabla^4 U \tag{4}$$

Then the energy equation is:

$$\frac{\partial T}{\partial t} + \vec{\mathrm{U}}(\nabla T) = \frac{1}{\mathrm{Pe}}(\nabla^2 T) \tag{5}$$

The instantaneous temperature T is decomposed into a base temperature $T_0(y)$ and the computational temperature components $T_{\mathrm{c}}(x, y, t)$ are:

$$T(x,y,t) = T_0(y) + T_{\mathrm{c}}(x,y,t) \tag{6}$$

For numerical simulation of nanofluids it is assumed that the continuum assumption is still valid for fluids with suspended nano size particles [8]. Thus, eqs. (4) and (5) can be written:

$$\frac{\partial \nabla^2 \vec{\mathrm{U}}}{\partial t} = -\nabla \times (\nabla \times \vec{\mathrm{H}}) + \frac{1}{\mathrm{Re}_{\mathrm{nf}}}\nabla^4 \vec{\mathrm{U}} \tag{7}$$

$$\frac{\partial T}{\partial t} + \vec{\mathrm{U}}(\nabla T) = \frac{1}{\mathrm{Pe}_{\mathrm{nf}}}(\nabla^2 T) \tag{8}$$

where

$$\frac{1}{\mathrm{Re}_{\mathrm{nf}}} = \frac{\mu_{\mathrm{nf}}}{\rho_{\mathrm{nf}} U_{\mathrm{in}} b_{1/2}}$$

It is assumed that the inlet mass flow rate is constant and Reynolds number changes with nanofluid viscosity:

$$\frac{1}{\mathrm{Pr}_{\mathrm{nf}}} = \frac{k_{\mathrm{nf}}}{\mu_{\mathrm{nf}} c_{p(\mathrm{nf})}} \qquad \text{and} \qquad \mathrm{Pe}_{\mathrm{nf}} = \mathrm{Pr}_{\mathrm{nf}}\,\mathrm{Re}_{\mathrm{nf}}$$

The specific heat was calculated with correlation as proposed by Pak and Cho [23]:

$$(c_p)_{\mathrm{nf}} = (1-\varphi)(c_p)_{\mathrm{bf}} + \varphi(c_p)_{\mathrm{p}} \tag{9}$$

The effective conductivity is calculated according to equation which is introduced by Yu and Choi [19]:

$$k_{\mathrm{nf}} = \left[\frac{k_{\mathrm{p}} + 2k_{\mathrm{bf}} + 2(k_{\mathrm{p}} - k_{\mathrm{bf}})(1+\beta)^3\varphi}{k_{\mathrm{p}} + 2k_{\mathrm{bf}} - (k_{\mathrm{p}} - k_{\mathrm{bf}})(1+\beta)^3\varphi}\right]k_{\mathrm{bf}} \tag{10}$$

Normally $\beta = 0.1$ is used to calculate the thermal conductivity of nanofluid. For calculating viscosity two experimental correlations have been used:

$$\begin{aligned} &\frac{\mu_{\mathrm{nf}}}{\mu_{\mathrm{bf}}} = 1 + 0.025\varphi + 0.015\varphi^2 \qquad \text{for} \qquad Al_2O_3\text{-water} \\ &\frac{\mu_{\mathrm{nf}}}{\mu_{\mathrm{bf}}} = 1.013 + 0.092\varphi - 0.015\varphi^2 \qquad \text{for} \qquad TiO_2\text{-water} \end{aligned} \tag{11}$$

Boundary and initial conditions

Equation (4) is a fourth-order, partial differential equation, so it requires four boundary conditions. The u is specified at the inlet ($x = 0$) and the outlet boundaries ($x = L_x$). By using continuity equation, $\partial u/\partial x$ is also specified at the inflow and outflow boundaries:

$$\frac{\partial v}{\partial y} = -\frac{\partial u}{\partial x} \tag{12}$$

The convective boundary conditions are used to generate the Dirichlet boundary condition for both velocity components and temperature:

$$\frac{\partial \psi}{\partial t} = -c\frac{\partial \psi}{\partial x} \tag{13}$$

where ψ is replaced by each of the velocity components. Energy equation requires two temperature boundary conditions, known as Dirichlet boundary conditions. A uniformly distributed tangent hyperbolic mean velocity at all x stations is the initial condition. These initial conditions must then be allowed to wash out of the outlet boundary before performing any statistical analysis on the jet flow. In other words, any particle at the inlet ($x = 0$) must be allowed to leave the outlet boundaries ($x = L_x$). Summary:

$$\begin{aligned} &t = 0 \qquad U(x,y,0) = \frac{1}{\cosh^2 y}, \qquad T(x,y,0) = \frac{1}{\cosh^2 y} \\ &x = 0 \qquad U(y) = \frac{1}{\cosh^2 y}, \qquad T(y) = \frac{1}{\cosh^2 y} \\ &x = L_x \qquad \frac{\partial \psi}{\partial t} = -c\frac{\partial \psi}{\partial x} \qquad \text{for} \quad U \text{ and } T \\ &y = \pm\infty \qquad U = 0 \end{aligned}$$

Numerical method and validation

The spatially developing jet is solved in a domain with a finite extend in the streamwise direction and doubly infinite ($y \to \pm\infty$) in the major-gradient (MG) direction. A compact third order Runge-Kutta time differencing scheme developed by wray [24] is used to advance the computations in time. The derivatives in the streamwise direction are computed using the Pade' finite difference scheme developed by Lele [25]. The lower order schemes used a cotangent mapping given by:

$$y = -\lambda \operatorname{cotg}(\pi\zeta) \tag{14}$$

To map the doubly infinite physical domain $-\infty \leq y \leq \infty$ into the finite computational domain with the interval of $0 \leq \zeta \leq 1$. λ in eq. (14) is the stretching parameter of the mapping.

For code validations and numerical method please see our previous work [15]. Expect that the mean velocity and half width jet in laminar jet have an analytical solution that reported in references [22, 26]. Figures 2 and 3 show very good agreement between numerical solution in this work and analytical solution.

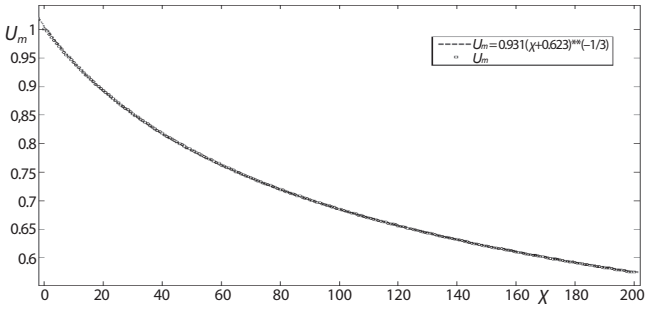

Figure 2. Mean velocity comparison between current work and analytical solution

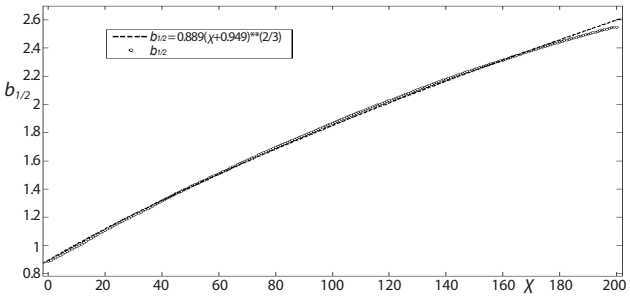

Figure 3. Jet half width comparison of the current work and analytical solution

Result and discussion

The case of 2-D Jet is studied in this work. The streamwise extent of computational domain is considered equal to 25 (L_x = 25) because the geometry of problem is unbounded and this amount is completely a logical one. The Reynolds number is Re = 100 for the laminar jet. Despite of temperature variation in this study, the Prandtl number is calculated equal to 6.2 for pure water and Prandtl sensitivity to temperature variation is neglected because of its complexity and also for time saving in numerical computations. The domain was discretised using 200 points to represent the stream wise x extend of the domain, 140 collocation points were used in the MG direction. A time step of 0.05 was used in this work.

Results for TiO_2-water

Figure 4 illustrates the relation between velocity time history at $x = 0.75L_x$, $y = 0$ and the solid volume fraction. When the solid volume fraction increases the nanofluid density increases too then at fixed mass flow rate (assumed in this paper) the velocity decreases via increasing the volume fraction. Figure 5 indicates the relation between temperature time history at $x = 0.75L_x$, $y = 0$, and solid volume fraction. Figure 6 exhibits the relation between solid volume concentra-

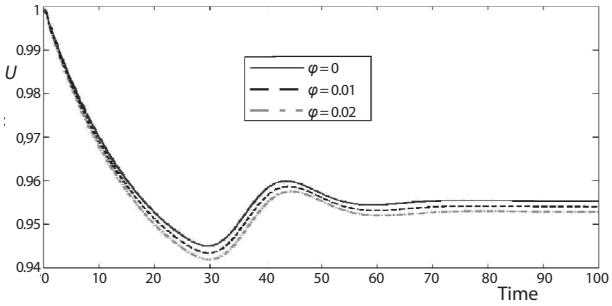

Figure 4. Velocity time histories for U component at $x = 0.75L_x$, $y = 0$

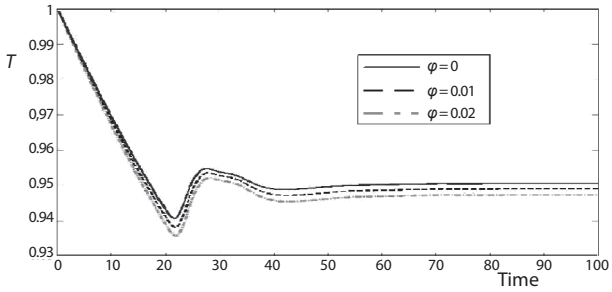

Figure 5. Temperature time histories at $x = 0.75L_x$, $y = 0$

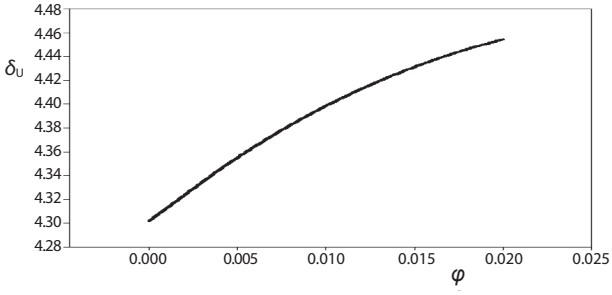

Figure 6. Effect of φ in δ_U at $x = 0.75L_x$, $t = 100$

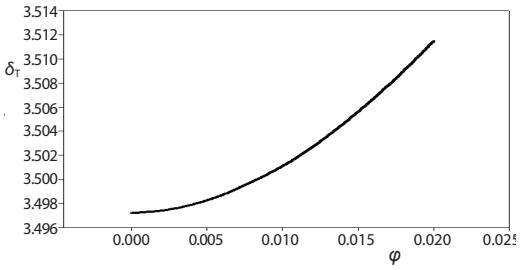

Figure 7. Effect of φ in δ_T at $x = 0.75L_x$, $t = 100$

tion and hydrodynamic cross-stream diffusion depth. The result shows an increase in hydrodynamic cross-stream diffusion depth when the solid volume fraction is increased. The velocity profile expands in each cross-stream section because of increasing the solid volume concentration and then hydrodynamic cross-stream diffusion depth increases via increasing solid volume fraction. With curve fitting we propose a lower limit for correlation that describe the relation between φ, and δ_U as:

$$\delta_U = \delta_{Uf} + 0.1534 \cdot \ln(\varphi + 0.1126) \quad (15)$$

Figure 7 illustrates the relation between the solid volume concentration and the thermal cross-stream diffusion depth. The result shows the thermal cross-stream diffusion depth increase when the solid volume fraction is increased. With curve fitting a lower limit for the correlation that describes the relation between φ, and δ_T as eq. (16) is proposed.

$$\delta_T = \delta_{Tf} + 0.0076\varphi + 0.3234\varphi^2 \quad (16)$$

Figure 8 shows the effect of solid volume fraction in U_{mean}. As shown in fig. 4 when the volume fraction increases the velocity at $y = 0$ decreases and the velocity profile expands in y-direction.

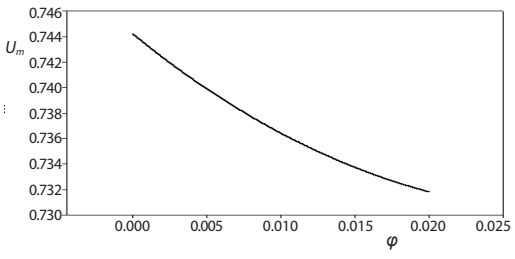

Figure 8. Effect of φ in U at $x = 0.75L_x$, $y = 0$ and $t = 100$

Results for Al_2O_3-water

The results show the manner for velocity and temperature time history for Al_2O_3-water is similar to TiO_2-water. Figure 9 exhibits the relation between solid volume concentration and hydrodynamic cross-stream diffusion depth. The result shows an increase in hydrodynamic cross-stream diffusion depth when the solid volume fraction is increased. Such as shawn in TiO_2 nanofluid. With curve fitting we propose a lower limit for correlation that describe the relation between φ and δ_U as:

$$\delta_U = \delta_{Uf} + \frac{0.35\left[\exp(6.118\varphi) - 1\right]}{6.118} \tag{17}$$

Figure10 illustrates the relation between the solid volume concentration and the thermal cross-stream diffusion depth. The result shows the thermal cross-stream diffusion depth increases when the solid volume fraction is increased. With curve fitting a lower limit for the correlation that describes the relation between φ and δ_T as eq. (18) is proposed:

$$\delta_T = \delta_{Tf} + 0.0196\left[1 - \exp(-3.8619\varphi)\right] + 0.0198\left[1 - \exp(-3.8619\varphi)\right] \tag{18}$$

Figure 11 shows the effect of solid volume fraction in U_{mean}.

Results of two different nanoparticles

Figure 12 illustrates the variation of Reynolds number varies with change in the solid volume fraction. The rate of decrease in Reynolds number with respect to addition of TiO_2 is greater than the rate of decrease with addition of Al_2O_3 nanoparticle. This is because the rate of increase in viscosity with any addition of TiO_2 is greater than the rate of increase of Al_2O_3 ad-

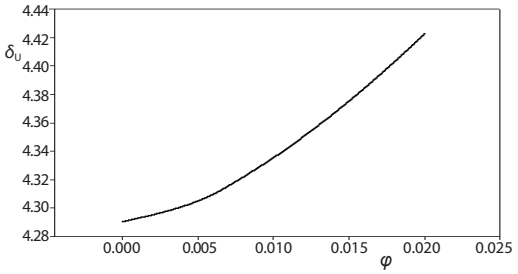

Figure 9. Effect of φ in δ_U at $x = 0.75L_x$, $t = 100$

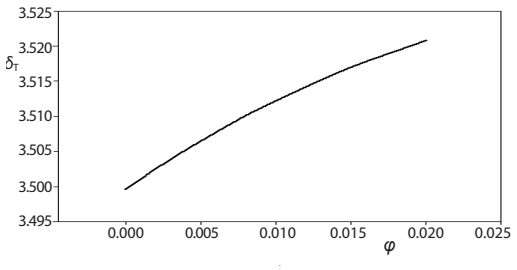

Figure 10. Effect of φ in δ_T at $x = 0.75L_x$, $t = 100$

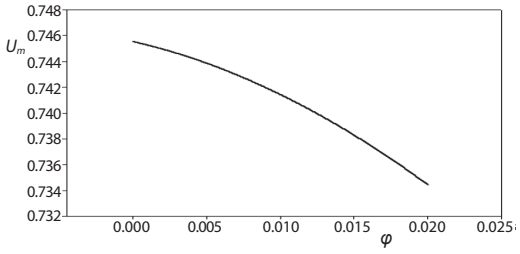

Figure 11. Effect of φ in U at $x = 0.75L_x$, $y = 0$ and $t = 100$

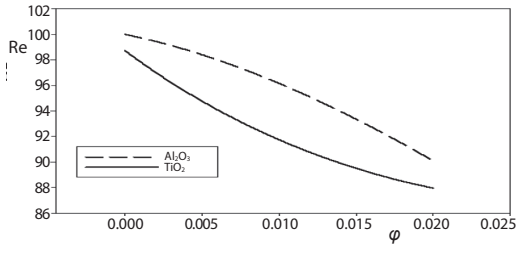

Figure 12. Reynolds number *vs.* φ

dition. Figure 13 shows the effect of TiO_2 nanoparticle volume fraction and Al_2O_3 nanoparticle volume fraction with respect to Peclet number. That's because the ratio of $(\rho c_p/k)_{nf}$ in TiO_2-water is greater than that of Al_2O_3-water. Figure 14 shows the effect of solid volume fraction in δ_U in two nanofluids. In TiO_2-water with any increase in φ the decrease in Reynolds number is much more experienced than Al_2O_3-water. Thus the δ_U in TiO_2-water is greater than that in Al_2O_3-water. Figure 15 shows the effect of solid volume fraction in δ_U for two nanofluids. In Al_2O_3-water with any increase in φ the decrease in Peclet number is much more experienced than TiO_2-water. Thus the δ_T in Al_2O_3-water is greater than that in TiO_2-water. Figure 16 shows the effect of solid volume fraction in U_{mean}.

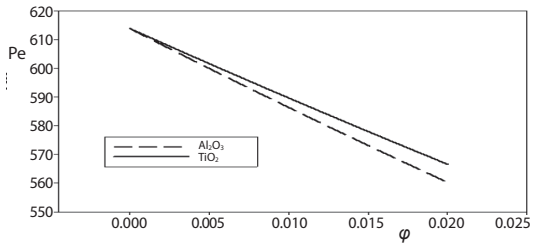

Figure 13. Peclet number *vs.* φ

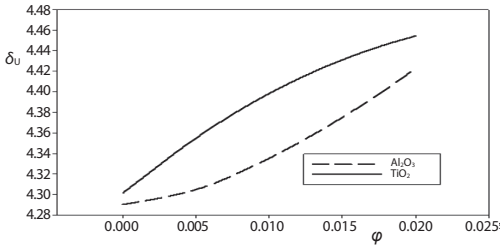

Figure 14. Effect of φ in δ_U at $x = 0.75L_x$, $t = 100$

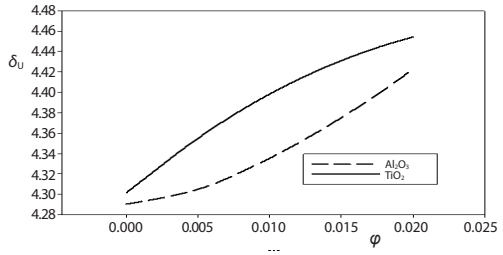

Figure 15. Effect of φ in δ_U at $x = 0.75L_x$, and $t = 100$

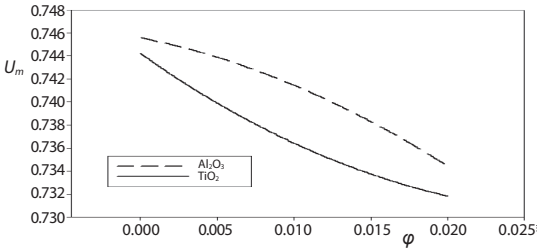

Figure 16. Effect of φ in U at $x = 0.75L_x$, $y = 0$ and $t = 100$

Conclusions

The two dimensional incompressible, spatially developing laminar nanofluid plane jet have been simulated in this work. A numerical method which employs a combination of compact finite difference and a mapped compact finite difference scheme are used to represent the spatial dependence of the jet flow. A compact finite difference was used to represent the solution in the streamwise direction and a mapped compact finite difference method was employed to describe the solution dependence in the major gradient direction. The simulations were time advanced by means of the third order Runge-Kutta method. The results for both nanofluids showed an increase in the cross stream thermal diffusion depth and cross stream hydraulic diffusion depth when the nanoparticle volume fraction increased. The mean velocity was decreased when solid volume fraction was increased for both nanofluids. In addition we compared the results between Al_2O_3-water and TiO_2-water nanofluids. In TiO_2-water with any increase in φ the decrease in Reynolds number is much more exprienced than Al_2O_3-water. Thus the δ_U in TiO_2-water is greater than that in Al_2O_3-water. In Al_2O_3-water with any increase in φ the decrease in Peclet number is much more experienced than TiO_2-water. Thus the δ_T in Al_2O_3-water is greater than that in TiO_2-water. The mean velocity in TiO_2-water is decreased more than in Al_2O_3-water.

Nomenclature

$b_{1/2}$ – half width of jet, [m]
c – advection speed of the large-scale structures, [ms^{-1}]
c_p – specific heat, [Jkg^{-1}K^{-1}]
k – thermal conductivity, [Wm^{-1}K^{-1}]
N_x – number of grid nodes in the direction, [–]
N_y – number of grid nodes in the direction, [–]
P – pressure, [Pa]
Pe – Peclet number, [–]
Pr – Prandtl number, [–]
Re – Reynolds number, [–]
T – instantaneous temperature, [K]
t – dimensionless time, [–]
U, V – dimensionless instantaneous velocity, [–]
u, v – dimensionless computational flow velocity component, [–]
x, y – dimensionless Cartesian co-ordinates, [–]

Greek symbols

δ – cross-stream diffusion depth, [m]
ζ – finite computational domain, [–]
λ – stretching parameter, [–]
μ – viscosity, [Pa·s]
ρ – density, [kgm^{-3}]
φ – nanofluid volume fraction, [–]
ψ – stream function, [–]
∇ – gradient operator, [–]

Subscripts

bf – basefluid
c – computational
nf – nanofluid
p – nanoparticle
T – thermal
U – hydrodynamic
0 – base and initial temperature-velocity
∞ – infinity

References

[1] Choi, S. U. S., Enhancing Thermal Conductivity of Fluids with Nanoparticles, *Developments and Applications of Non-Newtonian Flows*, *66* (1995), Oct., pp. 99-105
[2] Murshed, S. M. S., *et al*., Thermophysical and Electrokinetic Properties of Nanofluids – A Critical Review, *Applied Thermal Engineering*, *28* (2008), 17-18, pp. 2109-2125
[3] Santra, A. K., *et al*., Study of Heat Transfer Due to Laminar Flow of Copper-Water Nanofluid through Two Isothermally Heated Parallel Plate, *International Journal of Thermal Sciences*, *48* (2009), 2, pp. 391-400
[4] Kayhani, M. H., *et al*., Experimental Analysis of Turbulent Convective Heat Transfer and Pressure Drop of Al_2O_3/Water Nanofluid in Horizontal Tube, *Nanoletters*, *7* (2012), 3, pp. 45-54
[5] Nguyen, C. T., *et al.*, An Experimental Study of Confined and Submerged Impinging Jet Heat Transfer Using Al_2O_3-Water Nanofluid, *International Journal of Thermal Sciences*, *48* (2009), 2, pp. 401-411
[6] Kayhani, M. H., *et al.*, Experimental Study of Convective Heat Transfer and Pressure Drop of TiO_2-Water Nanofluid, *International Communications in Heat and Mass Transfer*, *39* (2012), 3, pp. 456-462
[7] Maghrebi, M. J., *et al*., Forced Convection Heat Transfer of Nanofluids in a Porous Channel, *Transport in Porous Media*, *93* (2012), 3, pp. 401-413
[8] Wang, X. Q., Mujumdar, A. S., Heat Transfer Characteristic of Nanofluid: A Review, *Internal Journal of Thermal Science*, *46* (2007), 1, 1-19
[9] Behzadmehr, A., *et al*., Prediction of Turbulent Forced Convection of a Nanofluid in Tube with Uniform Heat Flux Using a Two Phase Approach, *International Journal of Heat and Fluid Flow*, *28* (2007), 2, pp. 211-219
[10] Maiga, S. E. B., *et al.*, Heat Transfer Behaviors of Nanofluids in a Uniformly Heated Tube, *Superlattices and Microstructures*, *35* (2004), 3-6, pp. 453-462
[11] Heyhat, M. M., Kowsary, F., Effect of Particle Migration on Flow and Convective Heat Transfer of Nanofluids Flowing through a Circular Pipe, *ASME Journal of Heat Transfer*, *132* (2010), 6, 062401
[12] Talebi, F., *et al*., Numerical Study of Mixed Convection Flows in a Square Lid-Driven Cavity Utilizing Nanofluid, *International Communication in Heat and Mass Transfer*, *37* (2010), 1, pp. 79-90
[13] Shahi, M., *et al*., Numerical Study of Mixed Convective Cooling in a Square Cavity Ventilated and Partially Heated from the Below Utilizing Nanofluid, *International Communications in Heat and Mass Transfer*, *37* (2010), 2, pp. 201-213
[14] Lee, J., Mudawar, I., Assessment of the Effectiveness of Nanofluids for Single-Phase and Two-Phase Heat Transfer in Micro-Channels, *International Journal of Heat and Mass Transfer*, *50* (2007), 3-4, pp. 452-463

[15] Maghrebi, M. J., *et al*., Effects of Nanoparticle Volume Fraction in Hydrodynamic and Thermal Characteristics of Forced Plane Jet, *Thermal Science Journal*, *16* (2012), 2, pp. 455-468
[16] Luo, X. Y., *et al*., Numerical Study of MHD Effect on Liquid Metal Free Jet under Com-plex Magnetic Field, *Fusion Eng., 81* (2006), 8-14, pp. 1451-1458
[17] Konkachbaev, A., *et al*., Effect of Initial Turbulent Intensity and Velocity Profile on Liquid Jets for IFE Beam Line Protection, *Fusion Engineering*, *63-64* (2002), Dec., pp. 619-624
[18] Konkachbaev, A., Morley, N. B., Stability and Contraction of Rectangular Liquid Metal Jet in Vacuum Environment, *Fusion Engineering*, *51-52* (2000), Nov., pp. 1109-1114
[19] Yu, W., Choi, S. U. S., The Role of Interfacial Layers in the Enhanced Thermal Conductivity of Nanofluids: A Renovated Maxwell Model, *Journal of Nanoparticle Research*, *5* (2003), 1, pp. 167-171
[20] Nguyen, C. T., *et al.*, Temprature and Particle-Size Dependent Viscosity Data for Water-Based Nanofluids-Hysteresis Phenomenon, *International Journal of Heat and Fluid Flow*, *28* (2007), 6, pp. 1492-1506
[21] Duangthongsuk, W., Wongwises, S., Measurement of Temperature-Dependent Thermal Conductivity and Viscosity of TiO_2-Water Nanofluids, *Experimental Thermal and Fluid Science*, *33* (2009), 4, pp. 706-714
[22] Schilichting, H., *Boundary-layer Theory*, 8th ed., Springer-Verlag, Berlin, 2000
[23] Pak, B., Cho, Y., Hydrodynamic and Heat Transfer Study of Dispersed Fluids with Submicron Metallic Oxide Particles, *Experimental Heat Transfer*, *11* (1998), 2, pp. 151-170
[24] Wray, A., Hussaini, M. Y., Numerical Experiments in Boundary Layer Stability, *Proc. R. Soc. Lond. A.*, *392* (1984), 1803, pp. 373-389
[25] Lele, S. K., Compact Finite Difference Scheme with Spectral-Like Resolution, *Journal of Computational Physics*, *103* (1992), 1, pp. 16-43
[26] Armaghani, T., Maghrebi, M. J., DNS of Forced Incompressible Free Jet, 12th Fluid Dynamic Conference, *Proceedings*, Babol, Iran, 2009

Paper submitted: March 30, 2013
Paper revised: September 19, 2014
Paper accepted: September 20, 2014